

Comparison of MHD Stability between Positive- and Negative-Triangularity Tokamak Plasmas with Internal Transport Barriers^{*})

Yusai MASAMOTO, Nobuyuki AIBA¹⁾ and Masaru FURUKAWA

Tottori University, 4-101 Minami, Koyama-cho, Tottori-shi, Tottori 680-8552, Japan

¹⁾National institutes for Quantum and Radiological Science and Technology (QST), Naka, Ibaraki 311-0193, Japan

(Received 10 January 2022 / Accepted 9 March 2022)

Ideal magnetohydrodynamics (MHD) stability of tokamak plasmas is compared between positive and negative triangularity cross sections. The bootstrap current is included that is determined from the density and temperature profiles. This is crucial for a DEMO reactor design. The density and temperature profiles are chosen to have internal transport barriers (ITBs), which are necessary if an H-mode edge cannot be expected. The ideal MHD stability is examined in a wide range of the ITB position and the central temperature. We confirmed that ballooning modes are prone to be unstable when the ITB is located near the plasma edge for negative triangularity. Internal kink modes become dominant instability when the ITB is located inner side of the plasma for both positive and negative triangularities. We have succeeded to stabilize both ballooning and internal kink modes by introducing additional currents to control the safety factor profiles in a favorable manner.

© 2022 The Japan Society of Plasma Science and Nuclear Fusion Research

Keywords: DEMO reactor, internal transport barrier, negative triangularity, bootstrap current, ideal MHD stability

DOI: 10.1585/pfr.17.2403038

1. Introduction

Negative triangularity tokamak plasma was proposed for resolving an engineering challenge of the heat load on the divertor plates [1]. Since the negative triangularity of the plasma cross section is known to reduce the magnetic well, we may not be able to achieve favorable magnetohydrodynamics (MHD) properties. The ideal MHD stability properties in negative triangularity tokamak plasmas were numerically studied extensively by Medvedev *et al.* [2]. Their study assumed the pressure and current density profiles independently in the MHD equilibrium calculations. However, they are actually related through bootstrap current, and cannot be completely independent. Such a relation between the pressure and current density profiles must be taken into account especially in a DEMO reactor design since we have less control knob in it.

In our study, we compare ideal MHD stability properties between tokamak plasmas with positive and negative triangularity cross sections. Most importantly, we calculate the MHD equilibria with bootstrap current calculated from the density and temperature profiles.

Moreover, we assume pressure profiles with internal transport barriers (ITBs), which were not adopted in previous studies. Because of the reduced magnetic well especially at the plasma edge region in negative triangularity cases, we may not obtain an H-mode edge. In order to

achieve fusion power sufficient for a DEMO reactor, we should have ITBs. We assume L-mode edges in both positive and negative triangularity tokamak plasmas for fair comparisons.

As we will see, ballooning modes are prone to be unstable at the ITB region especially in the negative triangularity cases. We attempt to stabilize the ideal MHD modes including such ballooning modes by controlling the safety factor profile assuming an additional current drive. Note that we need to examine if electron cyclotron current drive (ECCD) or neutral beam injection (NBI) can realize the required current drive.

This paper is organized as follows. In Section 2, we briefly explain the codes used for the MHD equilibrium and linear ideal MHD stability analysis. Also we describe parameter settings in our research. In Section 3, we compare the stability calculation results between positive and negative triangularities. Moreover, we find how the instabilities can be stabilized by the additional current drive. Discussions and conclusions are given in the last section.

2. Methods

The MHD equilibrium is obtained by solving the Grad-Shafranov (G-S) equation

$$R^2 \nabla \cdot \left(\frac{\nabla \psi}{R^2} \right) = -\mu_0 R^2 \frac{dP}{d\psi} - F \frac{dF}{d\psi}, \quad (1)$$

where R is a radial coordinate in the cylindrical coordinates (R, ϕ, Z) , ψ is the magnetic flux function, P is the plasma

author's e-mail: m20j3049c@edu.tottori-u.ac.jp

^{*}) This article is based on the presentation at the 30th International Toki Conference on Plasma and Fusion Research (ITC30).

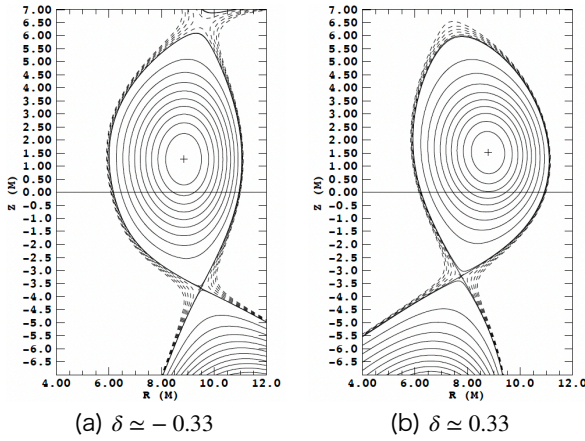


Fig. 1 Plasma cross sections.

pressure, $F := RB_\phi$ with B_ϕ being the toroidal magnetic field, and μ_0 is the vacuum permeability. The magnetic field is given by $\mathbf{B} = \nabla\phi \times \nabla\psi + F\nabla\phi$. The ACCOME code [3] and the MEUDAS code [4] are used for solving the G-S equation. The ACCOME code calculates the equilibrium using the bootstrap current density profile determined from the density and temperature profiles. The last term of Eq. (1) is expressed as

$$F \frac{dF}{d\psi} = -\mu_0 F \left(\frac{F}{\langle B^2 \rangle} \frac{dP}{d\psi} + \frac{\langle \mathbf{J} \cdot \mathbf{B} \rangle}{\langle B^2 \rangle} \right), \quad (2)$$

where the angular bracket represents a flux surface average. The parallel current term $\langle \mathbf{J} \cdot \mathbf{B} \rangle$ consists of bootstrap, Ohmic, NBI-driven, ECCD-driven, and additional currents. The NBI- and ECCD-driven currents are not considered in this study. The bootstrap current is calculated by Eq. (15) of Ref. [3]. It is based on the neoclassical theory by the moment approach of Hirshman-Sigmar [5].

The MARG2D code is used for linear stability analysis [6, 7]. MARG2D code determines ideal MHD stability of tokamak equilibria by solving an eigenvalue problem associated with the Newcomb equation

$$\mathcal{N}\mathbf{X} = -\lambda\mathcal{R}\mathbf{X}, \quad (3)$$

where \mathbf{X} is a vector of poloidal Fourier components of radial displacement, \mathcal{N} is a matrix representing two-dimensional Newcomb operator, \mathcal{R} is a matrix representing devised mass operator, and λ is the eigenvalue. The devised mass operator \mathcal{R} is chosen so that all λ are discrete eigenvalues.

In the following, parameter settings in our study are described. The parameters are based on JA DEMO 2014 [8]. The major radius is $R_0 = 8.5$ m, and the minor radius is $a = 2.5$ m. The ellipticity is $\kappa \approx 1.8$. The triangularities are chosen as $\delta \approx \pm 0.33$. Figure 1 shows the cross-sectional shapes of (a) the negative and (b) the positive triangularities. Note that the ellipticity and the cross-sectional area can be 5 - 10% different depending on the sign of the triangularity. We also assumed that a perfect conductive wall is located at 1.3 times the plasma minor radius.

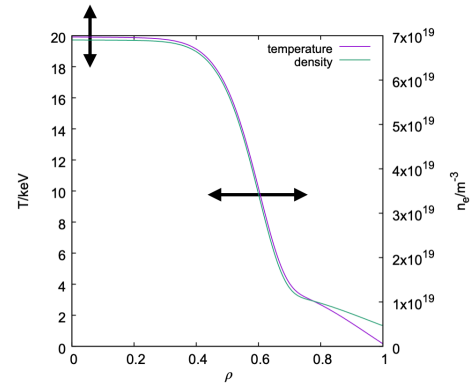


Fig. 2 An example of temperature and density profiles are shown as functions of the minor radius. The ITB positions and the central temperature are varied.

An example of temperature and density profiles is shown in Fig. 2. The horizontal axis is the minor radius $\rho := \sqrt{V/V_a}$, where V is the plasma volume inside a flux surface and V_a is at the plasma edge. We assumed ITBs in the temperature and density profiles, and varied their positions and the central temperature. The slope of the ITB was kept constant when the ITB positions are moved. The central temperature was changed every 5 keV. In this way, the relationship between the position of the ITB and the ideal MHD stability was investigated.

The total plasma current I_p is fixed at 10 MA, which is chosen different from [8] since the larger plasma current leads to lower safety factor and resultant internal kink instability in most cases of our survey. A bootstrap current is calculated from the density and temperature profiles, and the Ohmic current is introduced to adjust to 10 MA. In the latter part of this paper, an additional current will also be introduced, i.e., $I_{\text{Ohm}} = I_p - I_{\text{bs}} - I_{\text{add}}$.

3. Results

Initially, only the Ohmic current was considered except for the bootstrap current. We have calculated the ideal MHD stability index λ for toroidal mode numbers $n = 1, 2, 3, 4, 5, 10, 15, 20, 30$ and 50. Figure 3 shows the smallest λ among the selected toroidal mode numbers for (a) $\delta \approx -0.33$ and (b) $\delta \approx 0.33$, respectively, for various ITB position ρ_{ITB} which is the position where $dP/d\rho$ is maximum. The plasma is ideal MHD stable if $\lambda > 0$. In the range of $\rho_{\text{ITB}} < 0.45$, internal kink modes are unstable for both $\delta \approx \pm 0.33$.

The reason for the instability of the internal kink mode at small ρ_{ITB} is as follows. When the ITB is formed near the plasma center, amount of the bootstrap current decreases since the cross-sectional area decreases where the bootstrap current flows. Since the total current is fixed in this study, the Ohmic current increases that peaks at the center. Therefore, as the ITB is located closer to the magnetic axis, the safety factor at the center easily drops below 1, and the internal kink mode becomes unstable.

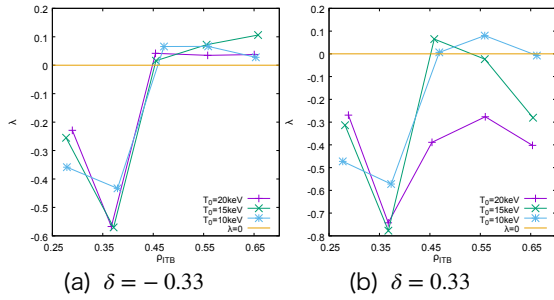


Fig. 3 Ideal MHD stability index λ ($\lambda \geq 0$ for stability) is plotted for various ITB positions ρ_{ITB} .

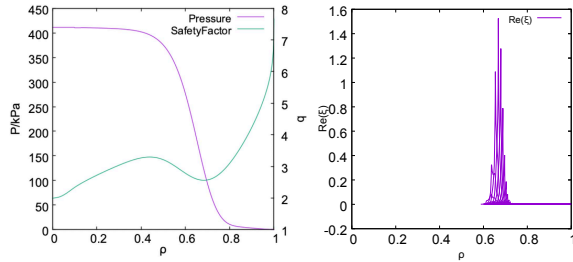


Fig. 4 A typical example of ballooning unstable case for $\delta \approx -0.33$. Pressure and safety factor profiles (left), and radial displacement of the ballooning mode (right).

As ρ_{ITB} is increased, ballooning modes become unstable when $\delta \approx -0.33$, while they are stable when $\delta \approx 0.33$. In the negative triangularity case, it becomes more unstable when the central temperature T_0 is increased. In the case of negative triangularity, the magnetic well decreases because the bad curvature region increases on the magnetic surface. As a result, the ballooning mode become easier to be destabilized.

Figure 4 shows a typical example of ballooning unstable case where $T_0 = 20$ keV and $\rho_{ITB} = 0.65$. The mode localizes in the ITB region.

Let us first consider stabilization of the ballooning modes by introducing an additional current. The key ingredient is to control the safety factor to have negative magnetic shear in the ITB region, where the eigenfunction localizes. This is realized by an additional current with its peak value at outer side than the ITB where the bootstrap current has its peak value. Figure 5 shows a typical example of the pressure, safety factor and current density profiles with and without the additional current. Without the additional current, the profiles with with $T_0 = 20$ keV and $\rho_{ITB} = 0.55$ are shown. Note that I_p was increased from 10 MA to 14 MA when the additional current is introduced since, mainly, the Ohmic current flows in the negative direction if the total current is not large enough. According to the increase of I_p , the normalized beta decreases significantly. Therefore T_0 is also increased to keep the normalized beta is kept unchanged. In addition to the case shown in Fig. 5, other cases with higher normalized beta than that without the additional current can also be successfully stabilized.

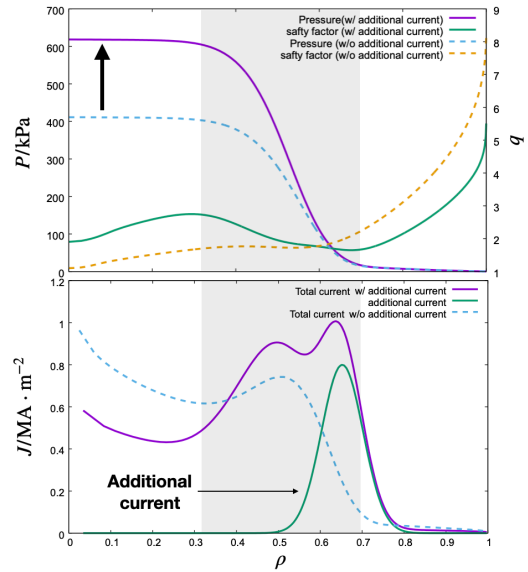


Fig. 5 Pressure, safety factor, and current density profiles. The dashed and solid curves show the profiles without and with the additional current, respectively.

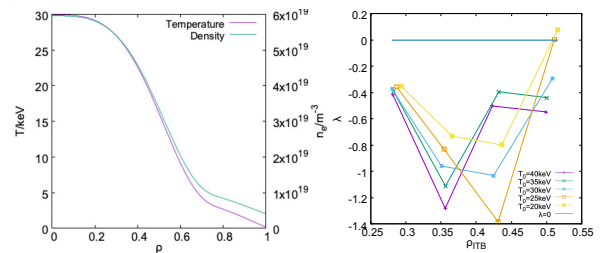


Fig. 6 Internal kink modes become unstable in a wider range of ρ_{ITB} for temperature and density profiles with gentler gradient at the ITBs (left). Ideal MHD stability index λ is shown for a range of ρ_{ITB} (right).

Let us now consider how to stabilize internal kink modes. The internal kink modes become unstable in a wider range of ρ_{ITB} when we adopt ITBs with gentler gradients than Fig. 2. Figure 6 shows the temperature and density profiles (left), and the corresponding stability index λ (right). By using these equilibrium temperature and density profiles, we tried to stabilize the internal kink modes. The strategy is to adjust the current density profile so that the safety factor does not fall below 1 by introducing additional currents. The resultant safety factor profiles are shown in Fig. 7. As a result, the internal kink modes are successfully stabilized in the present survey of parameter range.

When the safety factor profile is controlled to have reversed magnetic shear in the ballooning mode stabilization, there can exist multiple rational surfaces. A double kink mode [9] is known when two rational surfaces exist. The double kink mode has an eigenfunction with a top-hat shape; the radial displacement is finite in the region between two rational surfaces. We encountered a similar instability although the ballooning mode is stabilized. The

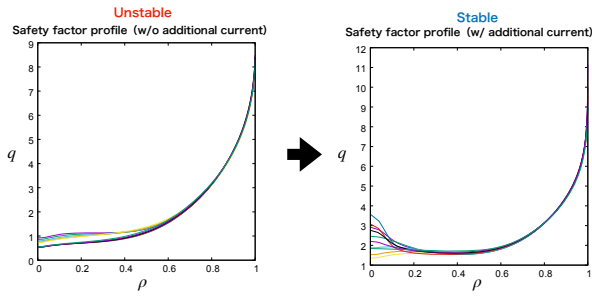


Fig. 7 Safety factor q profiles are adjusted so that $q > 1$ is realized by introducing additional currents for unstable cases with various T_0 and ρ_{ITB} .

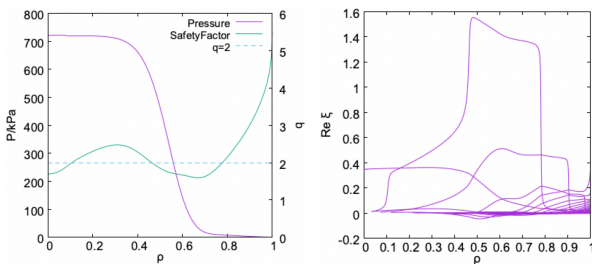


Fig. 8 Pressure and safety factor profiles at $T_0 = 35\text{keV}$ and $\rho_{\text{ITB}} = 0.55$ (left), and radial displacement of the mode (right). The poloidal mode number $m = 2$ component has the largest amplitude.

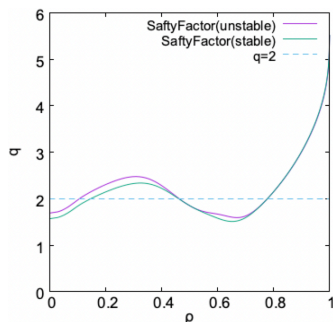


Fig. 9 Two safety factor profiles; one is stable and the other is unstable to double-kink-like mode.

equilibrium pressure and safety factor profiles as well as eigenfunctions are shown in Fig. 8. There are three $q = 2$ surfaces, and the mode has a similar structure as the double kink mode. The poloidal mode number $m = 2$ component has the largest amplitude between the $q = 2$ surfaces at $\rho \approx 0.4$ and 0.8 . The $m = 2$ component still have a finite amplitude in the range of $\rho \approx 0.1$ and 0.4 , which is different from the standard double kink mode.

We also found that this double-kink-like instability is sensitive to the small change of the safety factor profile. Figure 9 shows two safety factor profiles; one is stable but the other is unstable to the double-kink-like mode. We need to further examine what is the critical condition for this instability.

4. Discussion and Conclusions

The ideal MHD stability of tokamak plasmas is compared between positive and negative triangularity cross sections. We assumed ITBs in the temperature and density profiles, which are necessary for a DEMO reactor design with a negative triangularity cross section since we may not obtain an H-mode edge. The bootstrap current is calculated from the temperature and density profiles, which is crucial for the DEMO reactor design. It is confirmed that the ballooning mode is prone to be unstable when the triangularity is negative. Therefore, the negative triangularity operation at high beta should be stabilized by external controls. We have succeeded to stabilize the ballooning mode by controlling the safety factor profile by the additional current so that the magnetic shear becomes negative in the ITB region. The additional current is introduced with its peak value at outer side than the the ITB where the bootstrap current has its peak value. The internal kink mode can become unstable in both positive and negative triangularities when the ITB position is located at small minor radius. The mode can be stabilized also by the additional current to keep the safety factor above unity. The stabilization of ballooning and internal kink modes is achieved by controlling the safety factor profile, which is not related to the plasma boundary shape. Thus the one of the major advantages of the negative triangularity, i.e. the reduction of heat flux density on the divertor plates, will not be affected. Of course, the change of the safety factor profile may affect turbulent transport and thus the heat flux at the plasma edge, however, this is outside the scope of this study.

Acknowledgement

M.F. was supported by QST Research Collaboration for Fusion DEMO.

- [1] M. Kikuchi, 3rd WCI Symposium (Nov. 2012, KIST, Korea).
- [2] S. Yu. Medvedev, M. Kikuchi *et al.*, Nucl. Fusion **55**, 063013 (2015).
- [3] K. Tani, M. Azumi and R.S. Devoto, J. Comput. Phys. **98**, 332 (1992).
- [4] M. Azumi, G. Kurita, T. Matsumura, T. Takeda, Y. Tanaka and T. Tsunematu, Proc. 4th Int. Symp. on Comput. Methods Applied Sci. Engineering, Paris (North-Holland, Amsterdam, 1980), p. 335.
- [5] S.P. Hirshman and D.J. Sigmar, Nucl. Fusion **21**, 2079 (1981).
- [6] S. Tokuda and T. Watanabe, Phys. Plasmas **6**, 3012 (1999).
- [7] N. Aiba *et al.*, Comput. Phys. Commun. **175**, 269 (2006).
- [8] Y. Sakamoto, K. Tobita *et al.*, 25th IAEA Fusion Energy Conference (St. Petersburg, Russia, 2014) FIP/3-4Rb.
- [9] C.G. Gimblett, R.J. Hastie and T.C. Hender, Phys. Plasmas **3**, 3369 (1996).